Thermal behavior of mercury carboxylates as paintings' degradation products

Barannikov, R.; Vykydalova, A.; Bezdicka, P.; Hermans, J.; Plocek, J.; Svarcova, S.

DOI
10.1007/s10973-024-13463-3

Publication date
2024

Document Version
Final published version

Published in
Journal of Thermal Analysis and Calorimetry

Journal of Thermal Analysis and Calorimetry (2024) 149:13773–13784
https://doi.org/10.1007/s10973-024-13463-3

Thermal behavior of mercury carboxylates as paintings' degradation products

Ruslan Barannikov[1,2] · Anna Vykydalová[1,3] · Petr Bezdička[1] · Joen Hermans[4,5,6] · Jiří Plocek[1] · Silvie Švarcová[1]

Received: 1 December 2023 / Accepted: 8 July 2024 / Published online: 16 August 2024

Abstract

Mercury long-chain carboxylates have been identified recently as degradation products resulting from saponification occurring in painted artworks. Saponification belongs among the degradation processes endangering undesirably the appearance and stability of painted artworks, significant treasures of humanity. The mechanism of saponification has not been still fully understood because of the enormous complexity of both painting materials and factors triggering the deterioration. Moreover, the properties and stability of metal soaps resulting from this degradation are also poorly understood, complicating the choice of suitable conservation treatment. Relining, a heat-based restoration technique for reinforcing deteriorated canvases, can induce irreversible changes in paint layers, being applied inappropriately. Within this study, we report thermal behavior and stability of mercury palmitate ($Hg(C16)_2$), mercury stearate ($Hg(C18)_2$), and their respective mixtures with linseed oil in the temperature range of 25–150 °C, employing a combination of techniques, including DSC, TG-MS, FTIR, XRPD, and in situ high-temperature FTIR and XRPD. It was observed that while $Hg(C16)_2$ and $Hg(C18)_2$ undergo partial decomposition around 150 °C, in a mixture with linseed oil, they decompose rapidly at significantly lower temperature (around 100 °C). The decomposition of mercury carboxylates results in the formation of metallic mercury, a volatile toxic substance, and free fatty acids, reactants capable of further development of saponification in paint layers. In addition, a structural polymorph of $Hg(C16)_2$ and $Hg(C18)_2$ with a different arrangement of carboxylate groups around the mercury atom was formed after the heat treatment during the cooling down at ca 120 °C as documented by in situ high-temperature XRPD and FTIR.

Keywords Mercury carboxylate · DSC · TG-MS · FTIR · XRPD · HT-XRPD · Painting degradation

✉ Ruslan Barannikov
barannikov@iic.cas.cz

Anna Vykydalová
vykydalova@iic.cas.cz

Petr Bezdička
bezdicka@iic.cas.cz

Joen Hermans
j.j.hermans@uva.nl

Jiří Plocek
plocek@iic.cas.cz

Silvie Švarcová
svarcova@iic.cas.cz

[1] Institute of Inorganic Chemistry of the Czech Academy of Sciences, Husinec-Řež 1001, 250 68 Husinec, Czech Republic

[2] Department of Inorganic Chemistry, Faculty of Science, Charles University in Prague, Hlavova 2030/8, 128 43 Prague 2, Czech Republic

[3] Polymer Institute, Slovak Academy of Sciences, Dúbravská Cesta 9, 845 41 Bratislava, Slovakia

[4] Van 't Hoff Institute for Molecular Sciences, University of Amsterdam, PO Box 94157, 1090GD Amsterdam, The Netherlands

[5] Conservation and Restoration, Amsterdam School of Heritage, Memory and Material Culture, University of Amsterdam, PO Box 94552, 1090GN Amsterdam, The Netherlands

[6] Conservation and Science, Rijksmuseum, Hobbemastraat 22, 1071ZC Amsterdam, The Netherlands

Introduction

Metal carboxylates have attracted scientific interest due to their diverse applications in traditional and innovative technologies. They serve as additives for paint polymerization, or fungicide preparations, and/or act as precursors in various industrial processes [1, 2]. Besides this, heightened attention has been paid to metal carboxylates in the field of conservation science, particularly in the context of painting artworks' degradation resulting from pigment–binder interactions [3–8]. Among these processes, saponification (i.e., formation of long-chain metal carboxylates in paint layers) has been studied intensively for the last two decades because of its adverse effect on the paintings' appearance or structural coherence.

Generally, the formation of metal soaps in paint layers results from the reaction between metal cations from some pigments with fatty acids from binders; nevertheless, the mechanism is more complex. For example, in oil paintings, it involves an intricate evolution of carboxylates' species via ionomer to crystalline degradation products [9, 10]. The development of saponification is affected by various intrinsic factors, such as composition or combination of pigments and/or binders in the paint layers [7, 8, 11], and/or extrinsic factors, such as relative humidity, light exposure, temperature fluctuations, or conservation treatments [12, 13]. With respect to huge heterogeneity of paint layers as well as the enormous variety of environmental conditions, the saponification process and the role of particular factors have not been still fully understood. Moreover, the properties and behavior of neo-formed metal carboxylates in paintings under various condition have not been also clarified.

Besides prominently reported zinc [4–6, 14] and lead soaps [7, 11, 15–17], crystalline mercury soaps have been recently found in numerous miniature portraits [18], provoking the study of their crystal structure and properties [19]. The recent research has uncovered the potential of the red pigment cinnabar (HgS) to form crystalline mercury palmitate–stearates in egg-based tempera paints [19] or to affect the formation of lead carboxylates in multicomponent model paints [18, 20]. As part of our ongoing research into the crystallization of mercury carboxylates in drying oils, we have uncovered such thermal behavior that could imply potential risk of paintings containing cinnabar (vermilion) and/or mercury soaps derived from its degradation, especially during their exposure to elevated temperature caused, e.g., by intense lighting, heat radiation, temperature fluctuation during transportation or conservation treatment such as relining. Relining is a technique for reinforcement of degraded canvas based on ironing of a new canvas on the painting's reverse using various adhesives based on wax, resins, glue, or acrylates [21–23]. This treatment might cause irreversible changes in the artwork's appearance and stability [22, 24].

Various aspects of thermal behavior of different mercury carboxylates were reported in the past [25–29]. Within our previous study [19], we pointed out a contradiction with some reports on solid–solid transitions prior the solid–liquid transition for mercury palmitate and mercury stearate [25, 26]. Akanni et al. [27] reported the thermal decomposition of melted even chain length mercury carboxylates at temperatures above 180 °C.

Within this study, we demonstrate that the decomposition of mercury palmitate and stearate occurs at significantly lower temperature (around 100 °C) in the presence of linseed oil (commonly used painting binder) and that is complete in a relative short time (30 min) of heat treatment. This brings a risk, on the one hand, of conservators since the toxic mercury volatilizes during the treatment, and on the other hand, for paintings since the evolved free fatty acids can attack other pigments prone to saponification (e.g., zinc, lead, or mercury based). Furthermore, employment of the high-temperature in situ FTIR and XRPD experiments complementing the DSC and TG-MS analyses provides deeper insight into the phase transitions and decomposition process of the studied compounds and their mixtures with linseed oil.

Experimental

Sample preparation

Mercury palmitate $Hg(C16)_2$ and mercury stearate $Hg(C18)_2$ were synthesized in powder form as previously described elsewhere [16, 19]. The starting stoichiometric amount of carboxylic acids, namely palmitic acid (Fisher Scientific, pure) and stearic acid (Merck, pure) of the total amount 13 mmol, was dispersed in 200 mL of distilled water with addition of 2 mL of triethylamine (TEA, Fisher Scientific, pure). The suspension was dissolved into soluble TEA salts through vigorous stirring and heating at 65 °C. A stoichiometric amount of mercury acetate 6.5 mmol (Sigma-Aldrich, pure) was dissolved in 30 mL of water with 5 mL of acetic acid (Penta, pure), and this mixture was also heated to 65 °C under stirring. The mercury solution was then added dropwise to the TEA-carboxylate solution while maintaining intensive stirring. The temperature remained steady at 65 °C. A white sticky precipitate formed immediately. The suspension was heated for an additional hour at 65 °C before being left to cool to room temperature under continuous stirring overnight. All steps were carried out under a nitrogen atmosphere using decarbonized distilled water. Each sample underwent purification by dispersion in 15 mL of water, followed by centrifugation and decantation, repeated three

times. Finally, the samples were dried overnight at 75 °C in an air atmosphere.

During measurements, we utilized two distinct batches of mercury palmitate, both synthesized following above-mentioned procedures. For time-dependent ATR-FTIR measurements, we used a batch prepared in 2020 (*A*) while for the other experiments we used different one prepared later (*B*). This differentiation in batches does not impart any discernible impact on the behavior of mercury carboxylates, and it remains inconsequential to the core objectives of our experiments.

In the preparation of mixtures comprising mercury palmitate and/or stearate with linseed oil (LO), a consistent Hg-carboxylate:LO mass ratio of 1:3 was maintained. Each mixture consisted of 50 mg of the synthesized mercury carboxylate thoroughly mixed with 150 mg of linseed oil (Kremer Pigmente). The mixtures of mercury carboxylates with linseed oil were ground using a mortar and pestle to ensure a fine and homogeneous mixtures.

Differential scanning calorimetry (DSC)

DSC measurements of all samples were performed on Netzsch STA449 F1 Jupiter (Netzsch, Selb, Germany) equipped with an intracooler. Samples were measured in two parallels, while they were placed into an open alumina crucible, with mass around 10 mg. Argon was used as a purge gas. The flow was 50 mL min^{-1}. Each sample was heated from 40 to 140 °C at 2 °C min^{-1}, cooled down to 40 °C at 2 °C min^{-1}, and again heated up to 140 °C. Indium and zinc were used to calibrate the temperature. The criteria selected for determining the melting (T_m) and crystallization temperature (T_c) were based on the peak's onset. The enthalpies of melting (ΔH_m) and crystallization (ΔH_m^c) were obtained using the software Proteus61. In order to erase the sample's thermal history, the second heating cycle was used. This allows to impose a predetermined thermal profile on the sample, facilitating an assessment of the material's inherent properties. Through the second heating, the ultimate thermal characteristics of the cured sample were gained, enabling to differentiate between different batches of the material. The OriginPro software was used for data plotting in this and subsequent methods [30].

Thermogravimetry–mass spectrometry (TG-MS)

Thermogravimetry coupled with mass spectrometry was used to test the thermal stability of the material and to determine the released gas. All samples under study were measured by Netzsch STA449 F1 Jupiter (Netzsch, Selb, Germany) (TG) coupled with Agilent Technologies 5977B MSD (Agilent Technologies, Santa Clara, USA) (MS). The measurements of all samples were performed in parallels, and the samples were placed into an open alumina crucible with mass around 20 mg. Samples were heated to 110 °C over approximately 2.5 min and then maintained isothermally at 110 °C for 2 h followed by subsequent cooling. The entire process was conducted under synthetic air flow of 20 mL min^{-1}. Indium and zinc were used to calibrate the temperature. Specific fragments of analyzed gas were collected in multiple ion detection mode as intensity (A). Values of mass-to-charge ratios (m/z) were chosen depending on the composition of studied material. XRPD and FTIR measurements were done before and after thermal analysis (TA).

Fourier transform infrared spectroscopy (FTIR)

Infrared spectra of studied compounds were recorded by Nicolet Nexus 670 FTIR spectrometer equipped with a diamond crystal for attenuated total reflection (ATR). The spectra were recorded in the range of 400–4000 cm^{-1} with a resolution 4 cm^{-1}, number of scans 64. Spectra are not baseline corrected. Qualitative evaluation of acquired data was performed with Thermo Scientific OMNIC 9 v9.2.86 software for optical and/or vibrational spectroscopy.

Temperature-dependent ATR-FTIR spectroscopy was conducted using a PerkinElmer Frontier spectrometer equipped with a heatable diamond GladiATR module from Pike Technologies. Spectra were obtained as single scans at a resolution of 1 cm^{-1}, spanning a range from 4000 to 450 cm^{-1}. First, a background was recorded at 25 °C. A sample was then placed on the ATR crystal, after which it could be gradually heated to 150 °C and rapidly cooled using a pre-cooled brass heat sink. Throughout the process, spectra were collected with 5–6 spectra per minute.

To accurately determine the sample temperature during spectrum collection, we employed the linear relationship established between temperature and the background phonon signal of the diamond ATR crystal at 2155 cm^{-1}, as previously described by Hermans et al. [41] (Fig. S1, ESI†).

X-ray powder diffraction (XRPD)

Diffraction patterns were collected with a PANalytical X'PertPRO MPD diffractometer equipped with a conventional X-ray tube ($Co_{K\alpha}$ radiation, 40 kV, 30 mA, line focus) and a multichannel detector X'Celerator with an anti-scatter shield. X-ray patterns were measured in the range of 1.5 to 50° 2Θ with step of 0.0167° and 200 s counting per step. In this case, we used conventional Bragg–Brentano geometry with 0.02 rad Soller slit, 1/16° divergence slit, 1/8° anti-scatter slit, and 15-mm mask in the incident beam, 5.0-mm anti-scatter slit, 0.02 rad Soller slit, and Fe beta-filter in the diffracted beam. It represents a scan of about 80 min. XRD

patterns were not pre-treated before interpretation as no background correction was needed.

High-temperature diffraction patterns were collected with a PANalytical X'Pert PRO diffractometer equipped with a conventional X-ray tube ($Co_{K\alpha}$ radiation, 40 kV, 30 mA, line focus) and a multichannel detector X'Celerator with an anti-scatter shield. For experiments at elevated temperature, the high-temperature chamber (HTK 16, Anton Paar, Graz, Austria) was used. X-ray patterns were measured at 25 °C and between 30 °C 140 °C and vice versa with a step of 10 °C in the range of 5–26° 2Θ with a scan of about 11 min per temperature step.

Qualitative analysis was performed with the HighScore-Plus software package (Malvern PANalytical, The Netherlands, version 4.9.0) [31] and PDF-4+database [32].

Microscopic observation

Mercury palmitate $Hg(C18)_2$ was mixed with linseed oil according to the procedure discussed in "Sample preparation" Section. The mixture was dispensed in a Petri dish and subjected to a controlled thermal treatment at 150 °C for a duration of four hours in laboratory oven. Following this treatment, the sample was detailly examined using optical and scanning electron microscopes.

The optical microscope Arsenal (LPT 1513-T) equipped with Nikon PL L 40/0.60 160/0 lens was used for the initial analysis.

Subsequently, the scanning electron microscope Jeol JSM6510 is equipped with energy-dispersive spectrometer INCA (Oxford Instruments) with SDD detector capable of detecting elements heavier than Be at a resolution of 125 eV. The sample placed on a carbon support was analyzed in a high vacuum with accelerating voltage 10 kV with detection of secondary electrons (SEI). For the detection of backscattered electrons (BSE) and EDS acquisition low vacuum (50 Pa) with applied accelerating voltage of 20 kV was used.

Results and discussion

Differential scanning calorimetry measurements

Thermal properties, phase transitions, heat enthalpies, and compound purity of synthesized mercury carboxylates as well as starting carboxylic acids were examined by DSC. The DSC measurements of mercury palmitate and stearate (Fig. 1a and b) demonstrate well-defined intense peaks for both endothermic and exothermic processes in the range 120–130 °C, indicating a direct transition between the solid phase (*S*) and the liquid phase (*L*). This is in agreement with our previous study [19], while in contradiction with some reports on solid–solid transitions preceding shortly the solid–liquid transition for mercury palmitate and stearate [25, 26].

In the DSC data published by Adeosun et al. [25] for mercury palmitate and stearate, a solid phase–solid mesophase transition was observed for mercury palmitate as a strong signal at 110 °C and for mercury stearate as a weak signal detected around 82 °C. Ellis et al. [26] reported on the pre-melting transition of mercury palmitate and stearate. However, these transitions were overlapped with the melting transition for both mercury carboxylates. The pre-melting transition was only isolated for mercury stearate, and it occurred during slow cooling with a value around 111 °C. In our previous study [19], we suggested the weak DSC signals observed in the interval 50–60 °C corresponded to subtle structural changes in the crystal lattice detected by HT-XRPD. However, the signal may also originate from the presence of a small quantity of carboxylic acids, characterized by melting points falling within the 60–70 °C range (Fig. 1c and d). In the magnified insert of Fig. 1a and b, distinctive small broad peaks become evident, with an onset occurring around 60 °C. This observation deviates by approximately 10 °C from the values obtained for free fatty acids in this study. The melting transitions for both fatty acids are distinctly characterized by single melting peaks, with the onset occurring around 66 °C for palmitic acid and 73 °C for stearic acid. The compiled data, presented in Table 1, align favorably with previously reported melting temperatures and enthalpies for palmitic and stearic acids [33–36]. The shift of the melting and crystallization temperatures of fatty acids toward lower values can be ascribed to their presence in a mixture with carboxylates. The enthalpies of these peaks and the signal broadening are indicative of the relatively small concentration of these admixtures in synthesized mercury carboxylates.

The DSC curves of the first heating with respective values of T_m and ΔH_m are present in Fig. S2 and Table. S1 ESI†

$S_a \rightarrow L_a$ stands for additional phase transition ascribed to the minute contamination by fatty acids.

Thermal decomposition of mercury carboxylates

Time-dependent ATR-FTIR spectra of mercury palmitate recorded during heating up to 150 °C and subsequent cooling down back to room temperature (25 °C) show beside the melting and subsequent crystallization of the studied compound also a weak signal at 1700 cm^{-1} emerging during cooling at ca 125 °C (Fig. 2a). This signal can be assigned to the C=O stretch in free fatty acids. Following the treatment, no other bands related to palmitic acid's vibrations are apparent in the spectra, implying that the concentration of the newly formed palmitic acid is notably low. Furthermore, the intensities of antisymmetric and symmetric C=O stretching bands (1563 and 1343 cm^{-1},

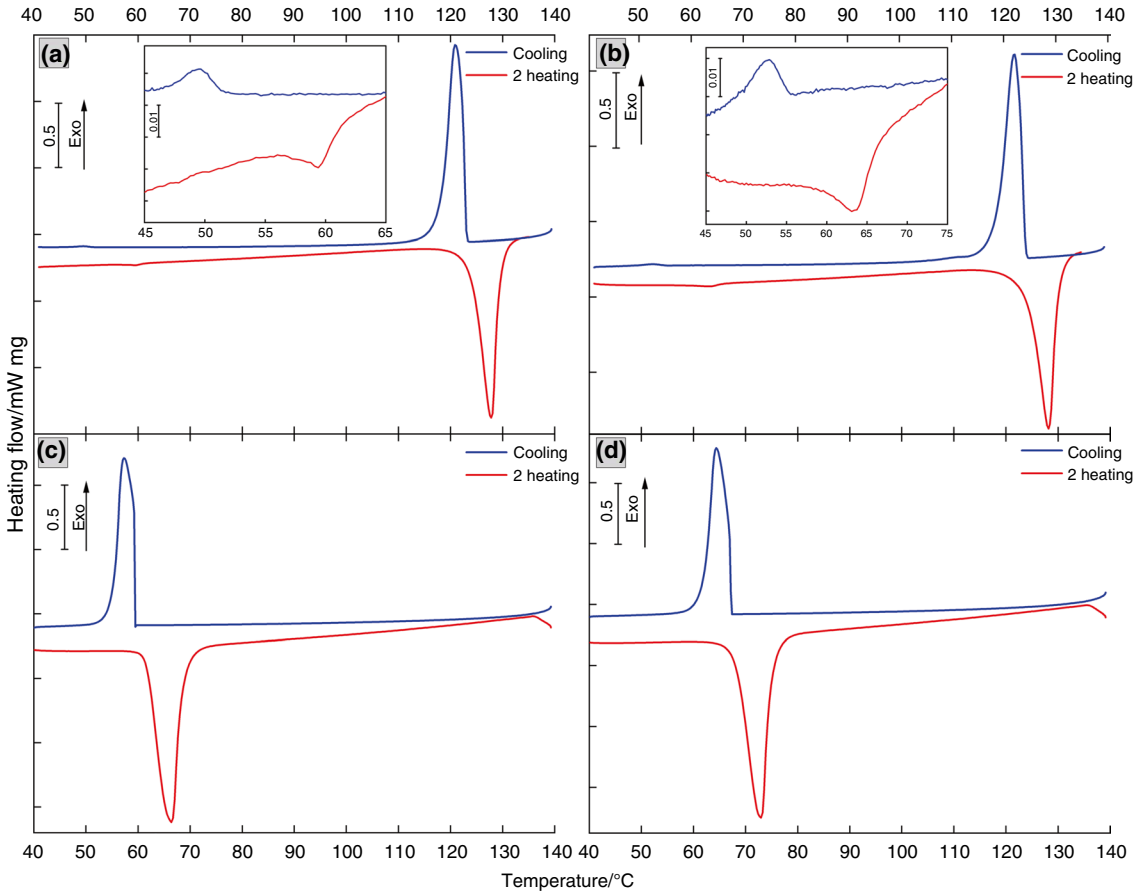

Fig. 1 DSC records of mercury palmitate (**a**), mercury stearate (**b**), palmitic acid (**c**), stearic acid (**d**)

Table 1 Values of melting temperatures (T_m), melting enthalpies (ΔH_m) and crystallization temperatures (T_c), crystallization enthalpies (ΔH_m^c) for studied metal carboxylates and free carboxylic acids

Sample	Phase transition	2nd heating		cooling	
		T_m/°C	ΔH_m/ J/g	T_c/ °C	ΔH_m^c/ J/g
$Hg(C16)_2$	$S_a \leftrightarrow L_a$	57.3	0.87	51.1	−0.68
	$S \leftrightarrow L$	123.9	160.1	123.1	−160.6
Palmitic acid	$S \leftrightarrow L$	66.4	176.8	57.3	−176.4
$Hg(C18)_2$	$S_a \leftrightarrow L_a$	60.5	1.92	55.1	−1.73
	$S \leftrightarrow L$	124.3	160.8	124.2	−158.4
Stearic acid	$S \leftrightarrow L$	73.0	191.7	64.4	−195.4

resp.) of mercury palmitate visibly decreased (Fig. 2b). Both together, these findings indicated partial decomposition of mercury palmitate under heating. This assumption can also explain the increase in melting enthalpies of free fatty acids during the second heating cycle in the DSC record for mercury carboxylates ascribed in Table 1 and Table S1. To elucidate the phenomenon, the detailed experiments were carried out using thermogravimetry coupled with mass spectrometry (TG-MS) and the complementing FTIR and XRPD measurements were performed before and after the thermal treatment to monitor changes in composition of studied carboxylates and/or their mixtures with linseed oil (LO).

Figure 3 represents isothermal measurements of $Hg(C16)_2$ and $Hg(C18)_2$, both with and without LO, at 110 °C under air atmosphere. Obviously, there is a significant difference between samples with and without LO. After 2 h of isothermal measurement, samples without LO underwent an approximate 1 mass % decrease, while samples with LO exhibited a greater reduction of ca 2 mass %. The mass decrease in samples without LO occurred steadily throughout the entire measurement period, whereas samples with LO exhibited a sudden mass decrease within the initial 20 min, followed by a more gradual decline. This observed effect correlates clearly with the evident release of mercury from the LO-containing system identified by detection of m/z 200.

To verify whether the observed mass loss corresponds to the decomposition of mercury carboxylates, further isothermal measurements of pure linseed oil were conducted at

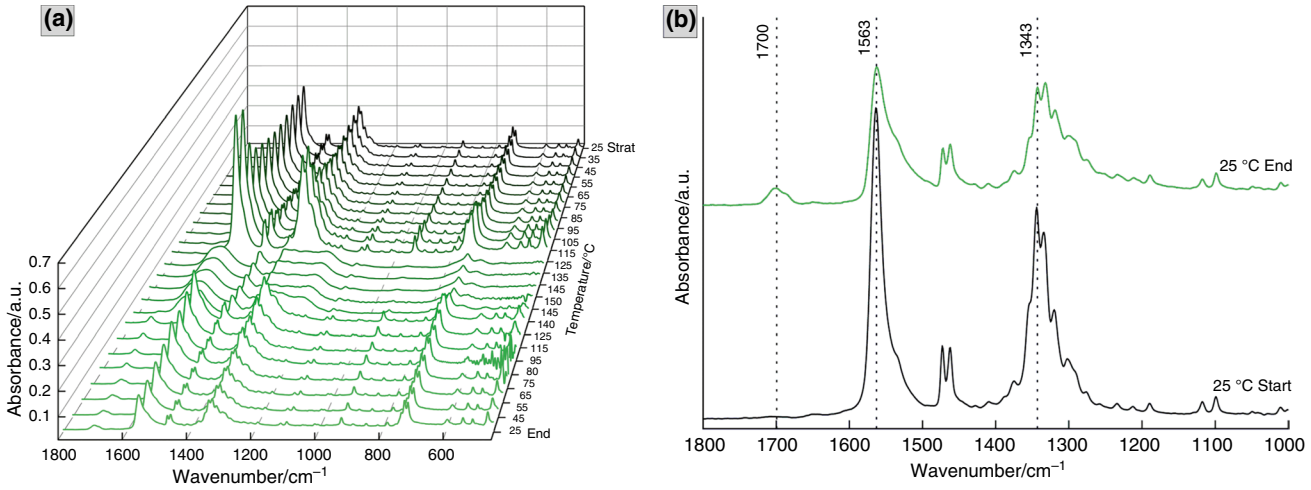

Fig. 2 Temperature-dependent FTIR spectra of mercury palmitate: measurement progression during heating/cooling cycles (**a**) and spectra before and after treatment (**b**)

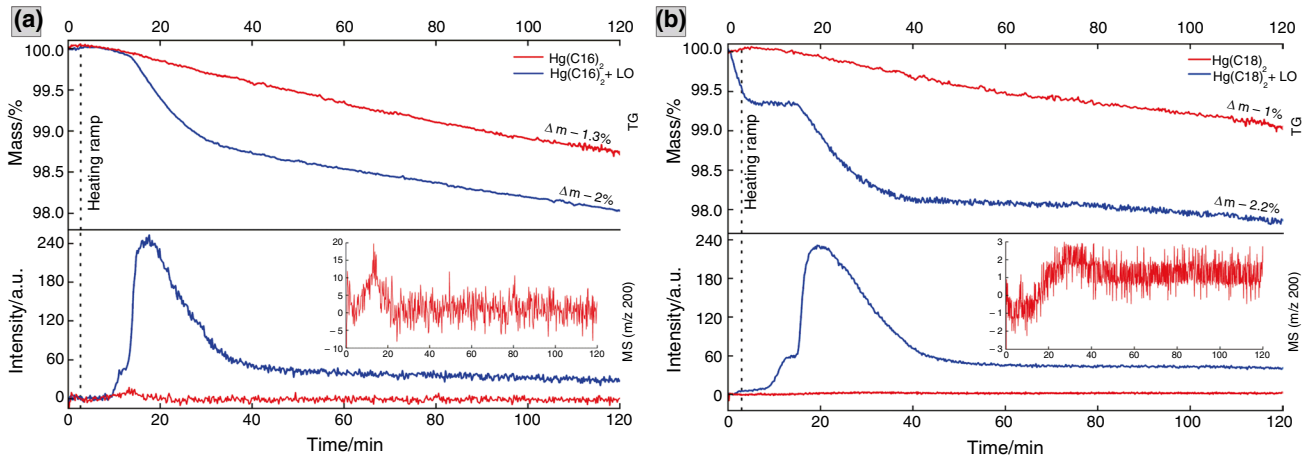

Fig. 3 Comparison of simultaneous TG-MS measurements of mercury palmitate (**a**) and mercury stearate (**b**) with linseed oil (blue curves) and without linseed oil (red curves) under synthetic air atmosphere

110 °C (Fig. S3 ESI†). The observed mass loss was approximately 0.2%.

Conversely, for samples without LO no detection of m/z 200 was observed, as indicated by a magnified MS spectrum (red curves in Fig. 3), revealing negligible peaks. The TG-MS measurements conclusively prove that mercury is released from the system consisting of mercury palmitate and/or stearate and linseed oil during the treatment even below the melting point of the both pure carboxylates in a relatively short time. This assertion finds further support in results obtained from FTIR and XRPD measurements (Fig. 4).

FTIR spectra and XRPD patterns of mercury palmitate, stearate, and their respective mixtures with LO, both before and after thermal analysis TA, are displayed in Fig. 4. In accordance with TG-MS, the significant changes in composition of samples with linseed oil are clearly apparent. The diffraction lines associated with both $Hg(C16)_2$ and $Hg(C18)_2$ disappeared completely after TA, while new diffraction lines corresponding to free palmitic and/or stearic acid appeared, indicating the complete decomposition of both carboxylates under formation of crystalline fatty acids (Fig. 4d and h). The XRPD patterns of mercury carboxylates without oil exhibit no significant deviations before and after thermal analysis (Fig. 4b and f).

The FTIR spectra of $Hg(C16)_2$ and $Hg(C18)_2$ mixed with LO recorded after TA corroborate the outlined process. The intense bands at 1563 cm^{-1} and 1343 cm^{-1} corresponding to the antisymmetric and symmetric C = O stretch vibrations of mercury carboxylates, respectively, disappeared. In their stead, well-defined new absorption bands arose at 1700 cm^{-1}, indicating an increase in free fatty acid

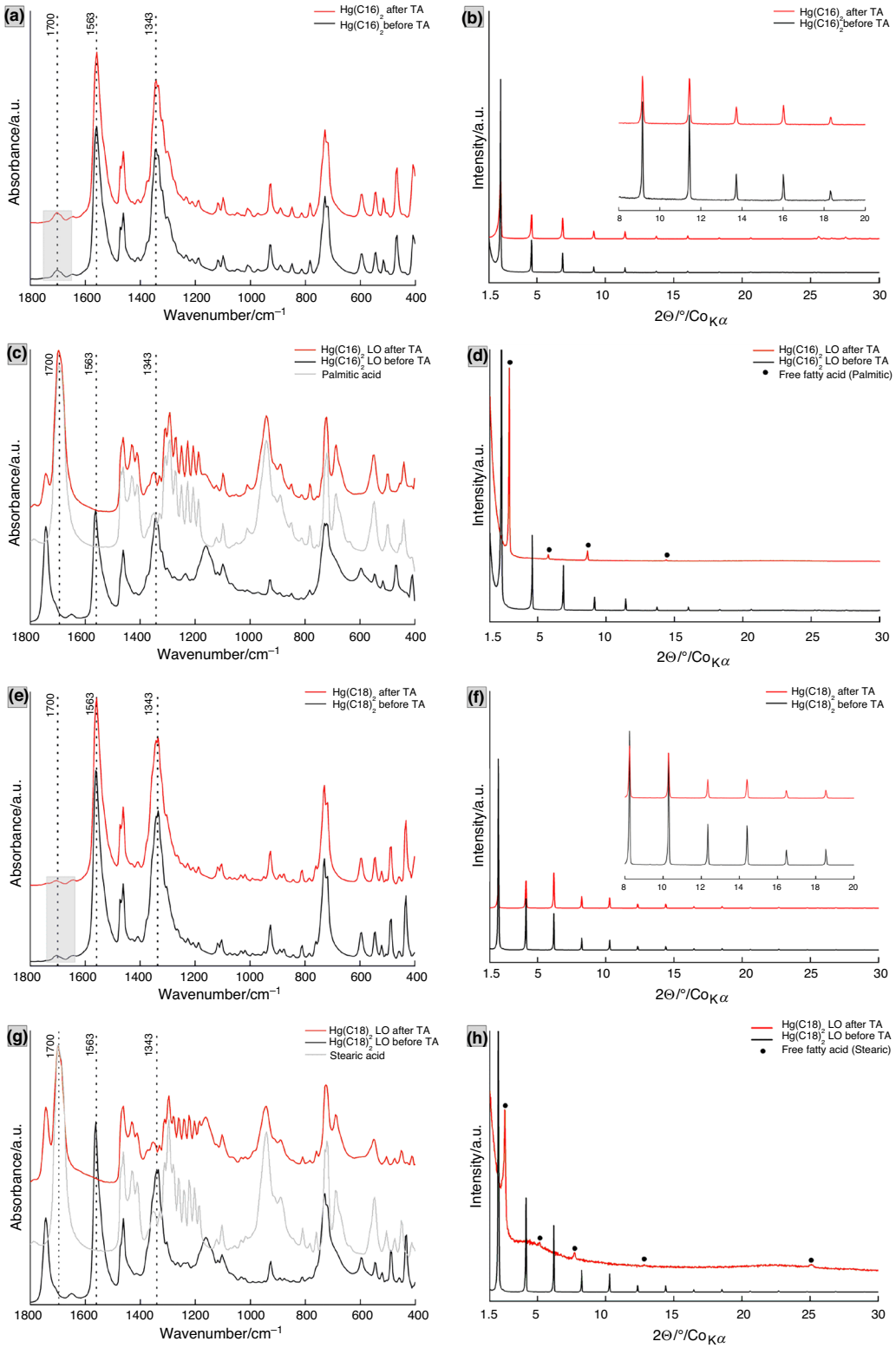

Fig. 4 FTIR spectra and XRPD patterns of mercury palmitate (**a**, **b**, resp.), the mixture of mercury palmitate with linseed oil (**c**, **d**, resp.), mercury stearate (**e**, **f**, resp.), the mixture of mercury stearate with linseed oil (**g**, **h**, resp.) before TA (black curves) and after TA (red curves); enclosed are the FTIR reference spectra (gray curves) and XRPD reference patterns (black dots) of fatty acids

concentration making visible all supplementary bands of palmitic acid (Fig. 4c and g).

In the FTIR spectra of both carboxylates without linseed oil, weak bands attributed to free carboxylic acids can be also observed; however, their intensity after TA has not changed (Fig. 4a and e). Considering earlier findings from DSC, where weak signals close to the melting points of carboxylic acids were detected (Fig. 1), we incline to assign these signals to minute fatty acids' contamination remained after the synthesis of the new batch (2.1, see Experimental). Apparently, in this case, the concentration of free fatty acid is very close to the detection limit of the XRPD method, and the intensities of its diffraction signals are indiscernible in comparison to the prominent main diffraction lines. The presence of this minute impurity has no effect on the observation of the above-described phenomena.

Thermal behavior of mercury carboxylates in a molten state was previously investigated for mercury palmitate at 200 °C [27] and stearate at 230 °C [29]. Both studies reported mercury soaps decomposition with considerable evolution of heat and release of metallic mercury, free carboxylic acid, alkene, and carbon dioxide as decomposition products. Akkani et al. [27] proposed a possible mechanism for the decomposition of mercury carboxylates, focusing on mercury decanoate, dodecanoate, tetradecanoate, and hexadecanoate. Using mercury dodecanoate as an illustrative example, it was suggested that heating the compound above its melting point up to 200 °C in a nitrogen atmosphere triggers the dissociation of the Hg–O bond. Simultaneously, the carboxylate anion attracts β-hydrogen, leading to the generation of metallic mercury, dodecanoic acid, carbon dioxide, and an alkene (undec-1-ene). This proposed mechanism aligns with our findings, as evidenced by the detection of mercury release by TG-MS, microscopic observations, and the identification of free fatty acids using FTIR and XRPD. However, within the techniques used, we did not detect carbon dioxide and the corresponding alkene.

In order to confirm the metallic mercury formation during mercury carboxylate decomposition, additional experiment was performed. The mixture of $Hg(C16)_2$ with linseed oil in a 1:3 ratio was placed in a Petri dish and subjected to a 150 °C treatment for four hours in a laboratory oven. After that, metallic mercury was observed within the oil film, as illustrated in photographs from both optical microscope and scanning electron microscope (Fig. S4, ESI†).

Notably, when mixed with linseed oil, mercury palmitate and stearate exhibited a more pronounced decomposition, releasing metallic mercury at significantly lower temperatures during heat treatment compared to pure mercury carboxylates. Since the melting temperature depends also on the concentration of a soap in linseed oil, we can assume its decrease with decreasing concentration similarly as reported by Hermans et al. for zinc and lead palmitates [5]. DSC measurements of $Hg(C16)_2$ in linseed oil (i.e., 25 mass % of $Hg(C16)_2$ in LO) provided in the supplementary (Fig. S5 ESI†) clearly indicate a shift in the melting point to lower values, approximately to 100 °C.

Additionally, the process might be influenced by the autoxidation of lipids occurring during the curing of linseed oil. Prior studies [8, 37–40] have reported the formation of peroxy (ROO·) radicals during the autoxidation of drying oils, generating a cascade of reactions producing free radicals and other reactive species attacking double bonds. Thus, the reason why we could not detect alkenes formed by decomposition of mercury carboxylates could lie in their rapid reaction with radicals formed by autoxidation of linseed oil.

High-temperature phase transitions of mercury carboxylates

Time-dependent ATR-FTIR measurements were performed for $Hg(C16)_2$ mixed with linseed oil. The sample was heated up to 150 °C and retained at this temperature with two distinct durations, 10 min and 30 min, to elucidate the impact of retention time on sample behavior. Initial and final spectra at 25 °C were labeled as *start* and *end*, respectively. In both samples heated for 10 min (Fig. 5a and b) and for 30 min (Fig. 5c and d), free palmitic acid was detected by the well-resolved signal at 1700 cm^{-1}, corresponding to the C = O stretching band. Other characteristic signals of palmitic acid within the range of 1800–450 cm^{-1} were also observed in the final spectrum, consistent with previous observations in "Thermal decomposition of mercury carboxylates" Section. Both measurements revealed distinctive changes, particularly in the asymmetric (1563 cm^{-1}) and symmetric (1343 cm^{-1}) stretching vibrations of the carboxylate group.

The final spectrum of 30-min sample at 25 °C (Fig. 5c and d) resembled that reported in "Thermal decomposition of mercury carboxylates" section after the TG-MS measurement (Fig. 4 c), indicating complete decomposition of mercury palmitate with the absence of carboxylate asymmetric at 1563 cm^{-1} and symmetric stretching vibrations at 1343 cm^{-1}.

In 10-min sample, some visible signals persisted in the carboxylate stretching vibrations region. The signals at 1563 cm^{-1} and 1343 cm^{-1} were not well resolved in a final spectrum (Fig. 5a and b), while newly formed signals at 1537 cm^{-1} and 1376 cm^{-1}, propagating with decreasing temperature, became clearly visible. Interestingly, these signals at 1537 cm^{-1} and 1376 cm^{-1} accompanied asymmetric and symmetric stretching vibrations in the initial spectrum. Considering lead carboxylates, where the main carboxylate asymmetric stretching vibration is accompanied by a shoulder representative for a specific coordination mode [17, 41], we suggest the signals at 1537 cm^{-1} and

1376 cm^{-1} correspond to mercury carboxylate stretching vibration modes with altered coordination. This suggestion finds support in the fact that in the 10-min sample, the signal at 1537 cm^{-1} and a novel signal at 1495 cm^{-1} (Fig. 5a and b) are well visible in the final spectrum, while in 30-min sample where mercury carboxylate was fully decomposed, the signals at 1538 cm^{-1} and 1499 cm^{-1} are missing in a final spectrum (Fig. 5c and d). The progression in Fig. 5c highlights the gradual formation and subsequent disappearance of these bands. Notably, after their disappearance, a visible drop was observed in the intensity of signal at 1376 cm^{-1}, possibly indicative for residual mercury carboxylate decomposition. As reported previously [42], mercury has potential to possess dual coordination modes to the oxygen atom—characteristic and effective. The characteristic one is represented by the very short bond distance in comparison with the effective one which is characterized by very long Hg–O bond distance. Thus, we can suppose that besides partial decomposition, a polymorph of mercury carboxylate with a different coordination environment is formed under the elevated temperature.

Complementing this assumption, in situ HT-XRPD of mercury palmitate (Fig. 6) illustrates the progression of diffraction patterns during heating to 140 °C and subsequent cooling. The observed drop in the intensity of main diffraction lines between 120 °C and 130 °C is caused by the melting, corresponding to the DSC observations. During the cooling process at 120 °C, the appearance of additional diffraction lines shifted slightly to higher 2Θ angles is apparent. As reported previously for lead carboxylates [17], a relatively small distinct difference of d-spacing could indicate the formation of a structural polymorph with different local arrangement around the central metal ion which is in agreement with the aforementioned results from time-dependent ATR-FTIR.

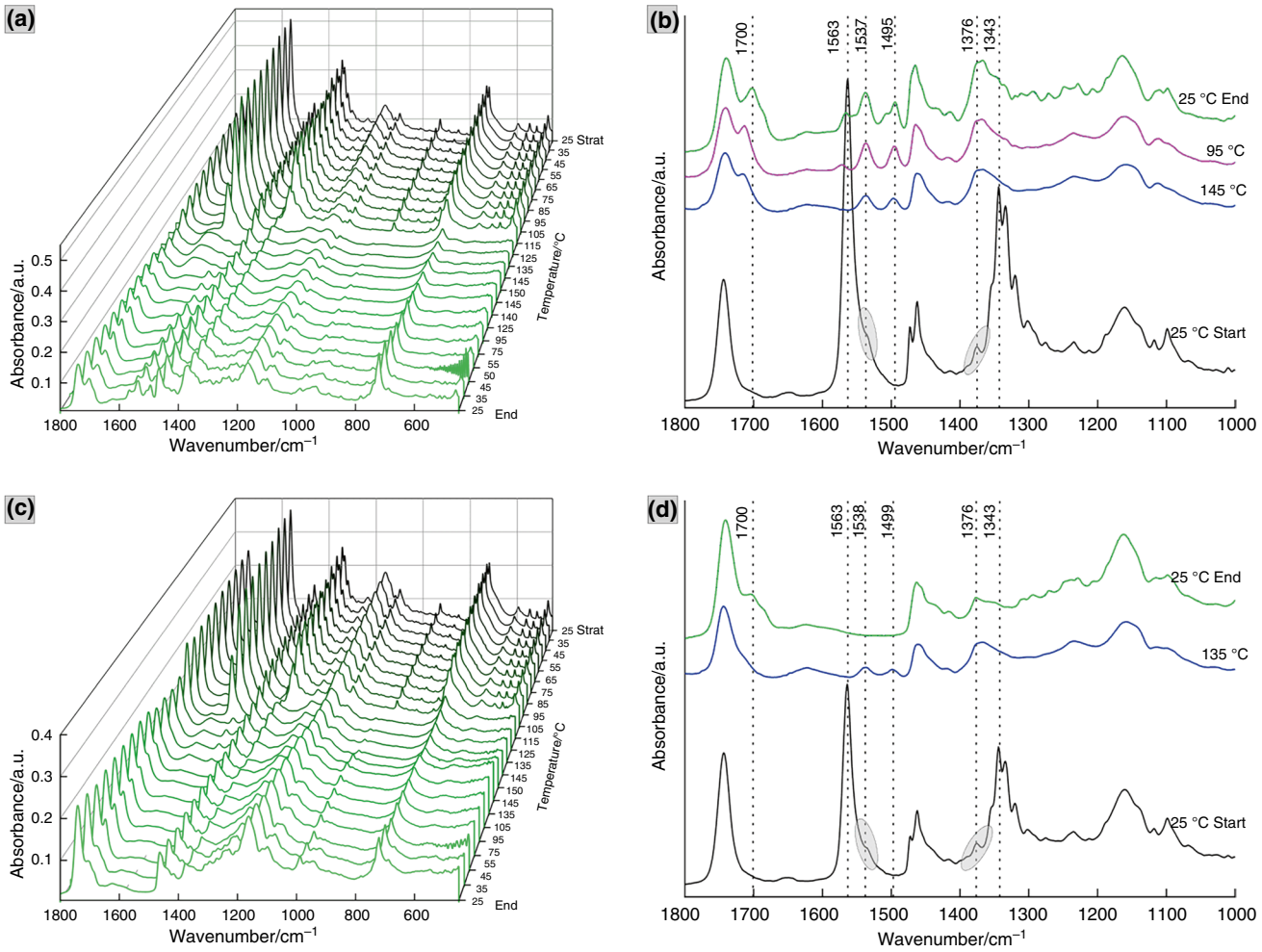

Fig. 5 Temperature-dependent FTIR spectra of mercury palmitate mixed with linseed oil: measurement progression during heating/cooling cycles and spectra before/after the treatment with 10 min retention at 150 °C (**a**, **b**, resp.) and with 30 min retention at 150 °C (**c**, **d**, resp.)

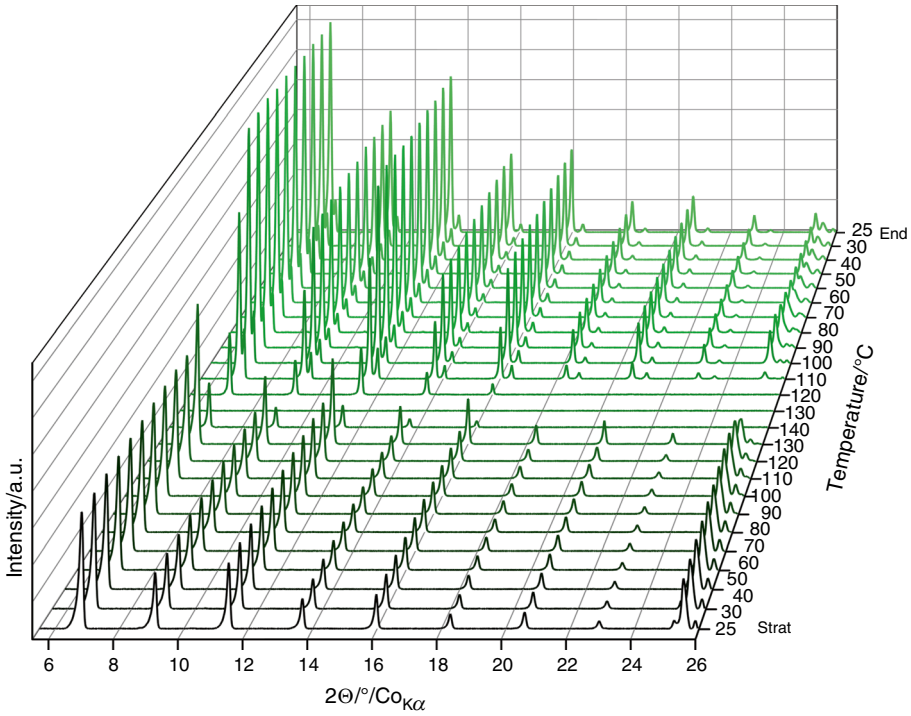

Fig. 6 In situ high-temperature XRPD patterns of powdered $Hg(C16)_2$

To further consider the influence of retention time on mercury palmitate decomposition, a supplementary experiment was performed in an isolated system, designed on a laboratory stirrer, ensuring a controlled and stable temperature (with a slight deviation ±0.5 °C). $Hg(C16)_2$ with LO placed in an alumina crucible was subjected to heating at 110 °C. The entire setup was insulated with isolation wool. Two samples were heated for duration of 10 and 30 min, with subsequent FTIR measurements performed before and after heating. The FTIR spectra of the 10 (Fig. S6a, ESI†) and 30-min retention (Fig. S6b, ESI†) time revealed discernable differences in the region of carboxylate stretching vibrations. The 10-min heating time resulted in trace signals in the carboxylate asymmetric and symmetric areas, while the 30-min spectra exhibit a complete absence of those bands, consistent with the aforementioned observations.

Thus, we can assume occurrence of two processes during the heat treatment: (1) partial or complete decomposition of mercury carboxylates dependent on the time retention and presence of linseed oil and (2) formation of structural polymorph with different coordination of carboxylate groups around mercury ion.

Conclusions

Within this study, we focused on the examination of thermal properties of mercury palmitate $Hg(C16)_2$ and mercury stearate $Hg(C18)_2$ which have been recently found as degradation products resulting from saponification of paint layers. The interest was driven by the preliminary assumption about thermal instability of these compounds which could bring a potential risk during the conservation treatment or handling of paintings at elevated temperature (e.g., relining).

Thermal behavior of $Hg(C16)_2$ and $Hg(C18)_2$ as well as their respective mixtures with linseed oil was studied in the temperature range between 25 and 150 °C using combination of techniques involving DSC, TG-MS, FTIR, XRPD, and in situ high-temperature FTIR and XRPD.

The melting temperatures of $Hg(C16)_2$, $Hg(C18)_2$, palmitic, and stearic acid determined by DSC are comparable to the previously reported values. On the other hand, only the solid–liquid phase transitions were detected in all studied compounds which is in contradiction with some previously published data for mercury carboxylates, reporting solid–solid transition shortly before their melting and suggesting the formation of a mesophase.

In contrast with available data on the thermal decomposition of mercury carboxylates for temperatures above 200 °C, we found that the partial decomposition of $Hg(C16)_2$ and $Hg(C18)_2$ occurred already during their heating below 150 °C as documented in the DSC records by the increased melting enthalpies of palmitic and/or stearic acids after the second heating cycle as well as by the signal of free fatty acid arising during the in situ high-temperature FTIR experiments.

The most important finding of the study lies, however, in the revealed effect of linseed oil's presence on the thermal stability of both studied mercury carboxylates. It was clearly manifested that decomposition of $Hg(C16)_2$

and $Hg(C18)_2$ occurred in the presence of linseed oil at substantially lower temperatures, being detected already around 100 °C, i.e., below the melting point of pure mercury carboxylates. The decomposition of mercury carboxylates results in the release of metallic mercury, a volatile toxic substance, and free fatty acids, compounds which can induce easily further development of saponification-related degradation in painted artworks. Therefore, these decomposition products represent a serious risk of deterioration of paintings as well as for restorers/conservators who would be exposed to toxic fumes. It is noteworthy that besides relatively low temperature, also the time necessary for a complete decomposition was relatively short, i.e., 30 min at 110 °C was sufficient for the complete decomposition of mercury palmitate mixed with linseed oil.

In addition, formation of a structural polymorphs of $Hg(C16)_2$ and $Hg(C18)_2$ *at elevated temperature* was detected by in situ high-temperature XRPD and FTIR experiments. From the character and position of diffraction lines and spectral bands, we deduce the change of coordination of carboxylate groups toward the mercury atom.

Supplementary Information The online version contains supplementary material available at https://doi.org/10.1007/s10973-024-13463-3.

Acknowledgements This work was supported by the Academy of Sciences of the Czech Republic within the frame of the research program Strategy AV21 No. 23—City as a Laboratory of Change; Historical Heritage and Place for Safe and Quality Life. The authors acknowledge the assistance provided by the Research Infrastructure NanoEnviCz, supported by the Ministry of Education, Youth, and Sports of the Czech Republic under Project No. LM2023066. A part of the study was performed at the University of Amsterdam during the research stay in the frame of the program ERASMUS+. The authors acknowledge colleague Pavla Kurhajcová for her assistance in the acquisition of FTIR spectra.

Funding Open access publishing supported by the National Technical Library in Prague. Ministerstvo Školství,Mládeže a Tělovýchovy,LM2023066,Akademie Věd České Republiky,Strategy AV21 No. 23,Silvie Svarcova

Declarations

Conflict of interest There are no conflicts of interest to declare.

References

1. Casadio F, Keune K, Noble P, Van Loon A, Hendriks E, Centeno SA, Osmond G. Metal soaps in art: conservation and research. Cultural heritage science. Cham: Springer; 2019. https://doi.org/10.1007/978-3-319-90617-1.
2. Van den Berg KJ, Bonaduce I, Burnstock A, Ormsby B, Scharff M, Carlyle L, Heydenreich G, Keune K. Conservation of modern oil paintings. Cultural heritage science. Cham: Springer; 2020. https://doi.org/10.1007/978-3-030-19254-9.
3. Gonzalez V, Fazlic I, Cotte M, Vanmeert F, Gestels A, De Meyer S, Broers F, Hermans J, Van Loon A, Janssens K, Noble P, Keune K. Lead (II) Formate in Rembrandt's Night Watch: detection and distribution from the macro- to the micro-scale. Angew Chem Int Ed. 2023;62: e202216478. https://doi.org/10.1002/anie.202216478.
4. Hermans JJ, Keune K, Van Loon A, Iedema PD, et al. Toward a complete molecular model for the formation of metal soaps in oil paints. In: Casadio F, et al., editors. Metal soaps in art. Cultural heritage science. Cham: Springer; 2019. https://doi.org/10.1007/978-3-319-90617-1_3.
5. Hermans JJ, Keune K, Van Loon A, Iedema PD. The crystallization of metal soaps and fatty acids in oil paint model systems. Phys Chem Chem Phys. 2016;18:10896. https://doi.org/10.1039/c6cp00487c.
6. Hermans JJ, Keune K, van Loon A, Stols-Witlox MJN, Corkery RW, Iedema PD. 2014 The synthesis of new types of lead and zinc soaps: a source of information for the study of oil paint degradation. ICOM-CC 17th Trienn Conf Prepr Melb. https://hdl.handle.net/11245/1.439706.
7. Švarcová S, Kočí E, Plocek J, Zhankina A, Hradilová J, Bezdička P. Saponification in egg yolk-based tempera paintings with lead-tin yellow type I. J Cul Her. 2019;38:8–19. https://doi.org/10.1016/j.culher.2018.12.004.
8. Švarcová S, Kočí E, Bezdička P, Garrappa S, Kobera L, Plocek J, Brus J, Šťastný M, Hradil D. Uncovering lead formate crystallization in oil-based paintings. Dalton Trans. 2020;49:5044–54. https://doi.org/10.1039/D0DT00327A.
9. Beerse M, Keune K, Iedema P, Woutersen S, Hermans J. Evolution of zinc carboxylate species in oil paint ionomers. ACS Appl Polym Mater. 2020. https://doi.org/10.1021/acsapm.0c00979.
10. Hermans JJ, Keune K, Van Loon A, Corkery RW, Iedema PD. Ionomer-like structure in mature oil paint binding media. RSC Adv. 2016. https://doi.org/10.1039/c6ra18267d.
11. Keune K, Boon JJ. Analytical imaging studies of cross-sections of paintings affected by lead soap aggregate formation. Stud Conserv. 2007;52(3):161–76.
12. Garrappa S, Kočí E, Švarcová S, Bezdička P, Hradil D. Initial stages of metal soaps formation in model paints: the role of humidity. Microchem J. 2020. https://doi.org/10.1016/j.microc.2020.104842.
13. Modugno F, Di Gianvincenzo F, Degano I, van der Werf ID, Bonaduce I, van den Berg KJ. On the influence of relative humidity on the oxidation and hydrolysis of fresh and aged oil paints. Sci Rep. 2019. https://doi.org/10.1038/s41598-019-41893-9.
14. Barman S, Vasudevan S. Melting of saturated fatty acid zinc soaps. J Phys Chem B. 2006. https://doi.org/10.1021/jp064306p.
15. Garrappa S, Hradil D, Hradilová J, Kočí E, Pech M, Bezdička P, Švarcová S. Non-invasive identification of lead soaps in painted miniatures. Anal Bioanal Chem. 2021. https://doi.org/10.1007/s00216-020-02998-7.
16. Kočí E, Rohlíček J, Kobera L, Plocek J, Švarcová S, Bezdička P. Mixed lead carboxylates relevant to soap formation in oil and tempera paintings: the study of the crystal structure by

complementary XRPD and ssNMR. Dalton Trans. 2019. https://doi.org/10.1039/c9dt02040c.
17. Martínez-Casado FJ, Ramos-Riesco M, Rodríguez-Cheda JA, Redondo-Yélamos MI, Garrido L, Fernández-Martínez A, Garcı´a-Barriocanal J, da Silva I. Lead (II) soaps: crystal structures, polymorphism, and solid and liquid mesophases. Phys Chem Chem Phys. 2017;19:17009. https://doi.org/10.1039/c7cp02351k.
18. Garrappa S, Bezdička P, Švarcová S, Hradilová J, Pech M, Hradil D. Non-invasive evidence of mercury soaps in painted miniatures on ivory. Eur Phys J Plus. 2023. https://doi.org/10.1140/epjp/s13360-023-03847-z.
19. Barannikov R, Kočí E, Bezdička P, Kobera L, Mahun A, Rohlíček J, Plocek J, Švarcová S. Long-chain mercury carboxylates relevant to saponification in oil and tempera paintings: XRPD and ssNMR complementary study of their crystal structures. Dalton Trans. 2022. https://doi.org/10.1039/d1dt04160f.
20. Garrappa S. Metal carboxylates as products of pigment-binder interactions in painted artworks, University of Chemistry and Technology Prague. 2022. Dissertation thesis
21. Ackroyd P, Phenix A, Villers C. Not lining in the twenty-first century: Attitudes to the structural conservation of canvas paintings. Conserv. 2002. https://doi.org/10.1080/01410096.2002.9995172.
22. Čermáková Z, Švarcová S, Hradilová J, Bezdička P, Lančok A, Vašutová V. Temperature-related degradation and colour changes of historic paintings containing vivianite. Spectrochim Acta A Mol Biomol Spectrosc. 2015. https://doi.org/10.1016/j.saa.2014.12.082.
23. Chiriu D, Pala M, Pisu FA, Cappellini G, Ricci PC, Carbonaro CM. Time through colors: a kinetic model of red vermilion darkening from Raman spectra. Dyes Pigment. 2021. https://doi.org/10.1016/j.dyepig.2020.108866.
24. Hackney S. Paintings on Canvas: Lining and Alternatives. in Tate Papers no.2, 2012. https://www.tate.org.uk/research/tate-papers/02/paintings-on-canvas-lining-and-alternatives, accessed 21 May 2024
25. Adeosun SO. A differential thermal analysis study of phase transitions in some mercury (II) carboxylates. J Therm Anal. 1978;14:235. https://doi.org/10.1007/BF01915161.
26. Ellis HA. Thermal Behaviour of Mercury(II) Carboxylates. Mol Cryst Liq Cryst. 1986. https://doi.org/10.1080/00268948608071766.
27. Akanni MS, Burrows D, Bay P. Product analysis, reaction mechanism and kinetics of the thermal decomposition of some even chain-length mercury(II) carboxylates. Thermochim Acta. 1984. https://doi.org/10.1016/0040-6031(84)85109-6.
28. Akanni MS, Abass NA. Solution behaviour in alcohols and phase transitions of cadmium (II), mercury (II) and lead (II) carboxylates. Liq Cryst. 1989;6:597. https://doi.org/10.1080/02678298908034179.
29. Lawrence ASC. The metal soaps and the gelation of their paraffin solutions. Trans Faraday Soc. 1938;34:660. https://doi.org/10.1039/tf9383400660.
30. OriginPro. Version 2021. OriginLab Corporation. Northampton, MA. USA.
31. Degen T, Sadki M, König EU, Nénert G. The HighScore suite. J Powder Diffr. 2014;29:S13–8. https://doi.org/10.1017/S0885715614000840.
32. PDF-5+ database. International Centre for Diffraction Data. Newtown Square, PA. U.S.A; 2023.
33. Acree WE. Thermodynamic properties of organic compounds: enthalpy of fusion and melting point temperature compilation. Thermochim Acta. 1991;189:37. https://doi.org/10.1016/0040-6031(91)87098-H.
34. Cedeño FO, Prieto MM, Espina A, García JR. Measurements of temperature and melting heat of some pure fatty acids and their binary and ternary mixtures by differential scanning calorimetry. Thermochim Acta. 2001;369:39. https://doi.org/10.1016/S0040-6031(00)00752-8.
35. Domalski ES, Hearing ED. Heat capacities and entropies of organic compounds in the condensed phase. Volume III. J Phys Chem Ref Data. 1996;25:1. https://doi.org/10.1063/1.555985.
36. Lide DR, Baysinger G, Chemistry S, Berger LI, Goldberg RN, Kehiaian HV. CRC handbook of chemistry and physics. Internet version 2005. Boca Raton: CRC Press; 2005.
37. Bonaduce I, Duce C, Lluveras-Tenorio A, Lee J, Ormsby B, Burnstock A, Van Den Berg KJ. Conservation issues of modern oil paintings: a molecular model on paint curing. Acc Chem Res. 2019;52:3397. https://doi.org/10.1021/acs.accounts.9b00296.
38. Meilunas RJ, Bentsen JG, Steinberg A. Analysis of aged paint binders by FTIR spectroscopy. Stud Conserv. 1990;35:33. https://doi.org/10.1179/sic.1990.35.1.33.
39. Rasti F, Scott G. The effects of some common pigments on the photo-oxidation of linseed oil-based paint media. Stud Conserv. 1980;25:145. https://doi.org/10.1179/sic.1980.25.4.145.
40. Baij L, Chassouant L, Hermans JJ, Keune K, Iedema PD. The concentration and origins of carboxylic acid groups in oil paint. RSC Adv. 2019;9:35559. https://doi.org/10.1039/C9RA06776K.
41. Hermans J, Zuidgeest L, Iedema P, Woutersen S, Keune K. The kinetics of metal soap crystallization in oil polymers. Phys Chem Chem Phys. 2021;23:22589. https://doi.org/10.1039/d1cp03479k.
42. Deacon GB, Phillips RJ. Relationships between the carbon-oxygen stretching frequencies of carboxylato complexes and the type of carboxylate coordination. Coord Chem Rev. 1980;33:227. https://doi.org/10.1016/S0010-8545(00)80455-5.